

Some Recent Developments in Auxiliary-Field Quantum Monte Carlo for Real Materials

Hao Shi^{1,2} and Shiwei Zhang^{1,3}

¹*Center for Computational Quantum Physics, Flatiron Institute, New York, NY 10010, USA*

²*Department of Physics and Astronomy, University of Delaware, Delaware, 19716, USA*

³*Department of Physics, College of William and Mary, Williamsburg, Virginia 23187, USA*

(Dated: 30 September 2020)

The auxiliary-field quantum Monte Carlo (AFQMC) method is a general numerical method for correlated many-electron systems, which is being increasingly applied in lattice models, atoms, molecules, and solids. Here we introduce the theory and algorithm of the method specialized for real materials, and present several recent developments. We give a systematic exposition of the key steps of AFQMC, closely tracking the framework of a modern software library we are developing. The building of a Monte Carlo Hamiltonian, projecting to the ground state, sampling two-body operators, phaseless approximation, and measuring ground state properties are discussed in details. An advanced implementation for multi-determinant trial wave functions is described which dramatically speeds up the algorithm and reduces the memory cost. We propose a self-consistent constraint for real materials, and discuss two flavors for its realization, either by coupling the AFQMC calculation to an effective independent-electron calculation, or via the natural orbitals of the computed one-body density matrix.

I. INTRODUCTION

The quantum many-body problem is one of the most challenging problems in the fields of condensed matter physics, quantum chemistry, and materials science. The properties of these systems result from the competition between the atomic environment, quantum delocalization of electrons, and electron-electron interaction. Accurate and reliable computations are essential for understanding and predicting the materials properties. The cost of finding the exact properties of these systems generally grows exponentially with the number of electrons and size of the systems, which motivates the development of modern numerical methods capable of approximate but sufficiently and systematically accurate solutions.

The most widely used numerical approaches for the many-body Schrodinger equation are based on density-functional theory (DFT)^{1,2}, which approximates the many-body effects by an auxiliary one-electron problem with an external potential. These approaches have been effective in most molecules and solids, and became the standard in electronic structure calculations. However, in the presence of strong electron-electron interaction, DFT-based approaches have not yet achieved the desired predictive power. Systematic approaches beyond independent-particle theories are intensely investigated for strongly correlated systems.

Numerical methods using Monte Carlo (MC) sampling techniques³⁻⁷ are promising in handling strongly-correlated electrons. These MC methods allow non-perturbative treatments beyond DFT and tend to scale well (low-power) with system size. However, in general there is a “sign” problem⁸⁻¹¹ for fermion systems, which arises from negative signs in the wave function under the interchange of two fermions. The sign problem manifests itself as the cancellation among the contributions of different MC samples, which becomes more severe as the system size is increased. In some cases, a phase problem appears which leads to more severe cancellations. Such cancellations cause the MC signal to decay exponentially versus noise. The unsolved sign problem and phase problem hinder the studies of the physics of many-fermion systems.

In this article, we discuss the auxiliary-field quantum Monte Carlo (AFQMC) method^{7,11-14} for real materials. This method controls the sign and phase problem by a constraint in the sign or gauge of path integrals in auxiliary-field space. It has demonstrated excellent versatility and accuracy across a wide range of systems and, in addition to lattice models, is being increasingly applied in molecules and solids. We present a self-contained description of

the method, providing a more unified framework between the formalisms for lattice models (short-range interaction), periodic solids with plane-waves, and molecular systems using quantum chemistry machinery. This formalism emphasizes a generic Hamiltonian form for AFQMC, and a treatment of the Hubbard-Stratonovich transformation that does not distinguish between discrete and continuous fields. It parallels a modern software library that we are developing which spans the multiple application domains. We discuss our advanced implementations to speed up the simulations and reduce the computational time, especially for multi-determinant trial wave functions. A self-consistent method is introduced which couples the AFQMC calculation to an independent-electron calculation to systematically improve the constraint.

II. METHOD

In this section we give a self-contained description of the AFQMC method. In AFQMC, the interaction part of the Hamiltonian is cast into a summation of non-interacting terms through a Hubbard-Stratonovich transformation. This is discussed in the form of a generic “Monte Carlo Hamiltonian” in the first and second parts. The summation is then sampled by random walks in the space of over-complete Slater determinants, which significantly reduces the sign problem. The projection and the random walk are outlined in the second and third parts, emphasizing the importance-sampling transformation in the language of a force bias which is independent of the detailed form of the auxiliary-fields (discrete or continuous). We then introduce the constrained path¹⁵ and phaseless⁷ approximation, which control the sign and phase problems to restore low-polynomial scaling, at the cost of losing exactness in the simulation.

A. Hamiltonian

The constrained-path and phaseless AFQMC methods have often been formulated in different flavors, depending on their target applications. These include, in addition to lattice models^{15,16} and Hartree-Fock-Bogoliubov approach¹⁷, several variants for realistic systems distinguished by the basis sets employed: solids with plane-wave basis^{7,18}, molecules with standard quantum chemistry basis sets of Gaussian type orbitals (GTOs)^{12,13}, and down-

folded Hamiltonians¹⁹ which treats solids but uses more of the GTO flavor of AFQMC. Here we seek to better unify the different flavors through a common starting point of an AFQMC calculation. The two forms of the Hamiltonian separately discussed below are the same, but re-expressing the original “*ab initio* Hamiltonian” into a “Monte Carlo Hamiltonian” allows us to introduce a more general discussion of the AFQMC algorithm and a more uniform framework to think about the algorithm and implementation.

1. *Ab initio* Hamiltonian

We start from the BornOppenheimer approximation^{20,21} for real materials. The first quantized Hamiltonian for many-electron systems is

$$\hat{H} = \sum_{i=1}^N \left[-\frac{1}{2} \nabla_i^2 + V_{ext}(r_i) \right] + \sum_{i<j}^N \frac{1}{r_{ij}}, \quad (1)$$

where r_i is the 3-dimensional coordinates of electron i , $r_{ij} = |r_i - r_j|$, and we have used atomic units.

The first part is the one-body term, which contains the kinetic energy and external potential, and the second part is the two-body term. Let us define $h(r) = -\frac{1}{2} \nabla^2 + V_{ext}(r)$ and $V(r_1, r_2) = \frac{1}{r_{12}}$. By choosing the appropriate basis $\phi_i(r)$, we can write the Hamiltonian into second-quantized form,

$$\hat{H} = \sum_{ij}^M \sum_{\sigma} h_{ij} a_{i\sigma}^{\dagger} a_{j\sigma} + \frac{1}{2} \sum_{ijkl}^M \sum_{\sigma\rho} V_{ijkl} a_{i\sigma}^{\dagger} a_{j\rho}^{\dagger} a_{k\rho} a_{l\sigma}, \quad (2)$$

with

$$h_{ij} = \int dr \phi_i^*(r) h(r) \phi_j(r), \quad (3)$$

and

$$V_{ijkl} = \int \int dr_1 dr_2 \phi_i^*(r_1) \phi_j^*(r_2) V(r_1, r_2) \phi_l(r_1) \phi_k(r_2). \quad (4)$$

Here we use M for the number of basis, $ijkl$ for the index of basis and $\sigma\rho$ for the index of spin. Note that V_{ijkl} has 4-fold symmetry,

$$V_{ijkl} = V_{jilk} = V_{klij}^* = V_{lkji}^*. \quad (5)$$

If the basis set is real, there will be the additional symmetry in V_{ijkl} , as is typically the case in quantum chemistry:

$$V_{ijkl} = V_{ikjl}. \quad (6)$$

2. Monte Carlo Hamiltonian

Auxiliary-field quantum Monte Carlo can be used for any Hamiltonian as long as it can be written into the form of a *Monte Carlo Hamiltonian*

$$\hat{H}_{\text{mc}} = \hat{T} + \frac{1}{2} \sum_{\gamma}^{\Gamma} \hat{L}_{\gamma}^2 + C, \quad (7)$$

where C is a real number, which is the nuclei repulsive energy for chemical systems. Both \hat{T} and \hat{L}_{γ} are one-body operators, whose general form is

$$\hat{O}_1 = \sum_{ij}^M \sum_{\sigma} O_{ij}^{\sigma} a_{i\sigma}^{\dagger} a_{j\sigma}. \quad (8)$$

Here \hat{O}_1 does not need to preserve symmetry between different spin components; it can be a color spin or a spinless operator for the corresponding systems.

There are a number of ways to transform an *ab initio* Hamiltonian into a Monte Carlo Hamiltonian, which can lead to AFQMC calculations of different efficiency or even systematic accuracy. The 4-rank tensor V_{ijkl} can be written into a matrix format by grouping $n = (il)$ and $m = (kj)$ index,

$$V_{ijkl} = V_{(il),(kj)} = V_{nm}, \quad (9)$$

which is a Hermitian matrix due to the symmetry in V_{ijkl} . For the most general case, a straightforward approach is diagonalizing the V_{mn} matrix,

$$V_{mn} = \sum_{\gamma} U_{m\gamma} D_{\gamma} U_{\gamma n}^{\dagger} \quad (10)$$

$$= \sum_{\gamma} \left(\sqrt{D_{\gamma}} U_{m\gamma} \right) \left(\sqrt{D_{\gamma}} U_{nr}^* \right) \quad (11)$$

$$= \sum_{\gamma} L_{m\gamma} L_{nr}^*. \quad (12)$$

This has a high cost and is not practical for large M .

For quantum chemistry applications, the most common approach has been using modified Cholesky decomposition²²⁻²⁵. Let us assume that we have already written the decomposition to the J^{th} step

$$V_{mn} = \sum_{\gamma}^J L_{m\gamma} L_{n\gamma}^* + \Delta_{mn}^J \quad (13)$$

$$= V_{mn}^J + \Delta_{mn}^J, \quad (14)$$

where Δ_{mn}^J is the reminder between V_{mn} and V_{mn}^J . We can generate the next Cholesky vector by

$$L_{m(J+1)} = \frac{\Delta_{m[n]_J}^J}{\sqrt{\Delta_{[n]_J[n]_J}^J}}, \quad (15)$$

with $[n]_J$ the index of largest diagonal elements of Δ_{mn}^J . If $\Delta_{[n]_J[n]_J}^J \leq \epsilon$, then all the elements

$$|V_{mn} - V_{mn}^J| = |\Delta_{mn}^J| \leq \epsilon. \quad (16)$$

Empirically, we choose $\epsilon \sim 10^{-6}$ for quantum chemical systems and the total number of Cholesky vectors, Γ , is around $10M$ after the truncation.

With the modified Cholesky decomposition, we can turn the *ab initio* Hamiltonian into

$$H = \sum_{ij}^M \sum_{\sigma} h_{ij} a_{i\sigma}^{\dagger} a_{j\sigma} + \frac{1}{2} \sum_{\gamma}^{\Gamma} \sum_{ijkl}^M \sum_{\sigma\rho} L_{(il)\gamma} L_{(kj)\gamma}^* a_{i\sigma}^{\dagger} a_{j\rho}^{\dagger} a_{k\rho} a_{l\sigma}. \quad (17)$$

After regrouping the index, we have

$$H = \sum_{ij}^M \sum_{\sigma} h_{ij} a_{i\sigma}^{\dagger} a_{j\sigma} - \frac{1}{2} \sum_{\gamma}^{\Gamma} \sum_{ijkl}^M \sum_{\sigma\rho} L_{(il)\gamma} L_{(kj)\gamma}^* a_{i\sigma}^{\dagger} (\delta_{jl} \delta_{\rho\sigma} - a_{l\sigma} a_{j\rho}^{\dagger}) a_{k\rho} \quad (18)$$

$$\begin{aligned} &= \sum_{ij}^M \sum_{\sigma} \left[h_{ij} - \frac{1}{2} \sum_{\gamma}^{\Gamma} \sum_k^M L_{(ik)\gamma} L_{(jk)\gamma}^* \right] a_{i\sigma}^{\dagger} a_{j\sigma} \\ &+ \frac{1}{2} \sum_{\gamma}^{\Gamma} \left(\sum_{il}^M \sum_{\sigma} L_{(il)\gamma} a_{i\sigma}^{\dagger} a_{l\sigma} \right) \left(\sum_{jk}^M \sum_{\rho} L_{(kj)\gamma}^* a_{j\rho}^{\dagger} a_{k\rho} \right) \end{aligned} \quad (19)$$

Equation (19) is a Monte Carlo Hamiltonian, with

$$\hat{T} = \sum_{ij}^M \sum_{\sigma} \left[h_{ij} - \frac{1}{2} \sum_{\gamma}^{\Gamma} \sum_k^M L_{(ik)\gamma} L_{(jk)\gamma}^* \right] a_{i\sigma}^{\dagger} a_{j\sigma}, \quad (20)$$

and

$$\hat{L}_{\gamma} = \sum_{il}^M \sum_{\sigma} L_{(il)\gamma} a_{i\sigma}^{\dagger} a_{l\sigma}. \quad (21)$$

Note that we have used the property that $L_{(il)\gamma} = L_{(li)\gamma}^*$ for systems with real basis functions.

Recently density-fitting²⁶ and low-rank tensor decomposition^{27,28} have also been adopted. For plane-wave calculations, the Coulomb repulsion is naturally bilinear in momentum space which can be decomposed analytically^{7,18}. And of course in lattice models with short-range interactions specialized decompositions can be used^{15,16}. All of these forms can be cast in the form of the Monte Carlo Hamiltonian, which we will use as the starting point of the AFQMC calculations below.

B. Projection

AFQMC solves the ground state Schrodinger equation by the imaginary-time projection

$$|\Psi_0\rangle \propto \lim_{\beta \rightarrow \infty} \left(e^{-\beta \hat{H}_{mc}} \right) |\Psi_I\rangle. \quad (22)$$

As long as the initial wave function is not orthogonal to the ground state wave function ($\langle \Psi_0 | \Psi_I \rangle \neq 0$), it will converge to the ground state when the imaginary projection time β approaches infinite. In practice, β is discretized into n small time slices, with a time step $\Delta\tau = \beta/n$. The projection can be evaluated as

$$|\Psi_0\rangle \propto \lim_{n \rightarrow \infty} \left(e^{-\Delta\tau \hat{H}_{mc}} \right)^n |\Psi_I\rangle. \quad (23)$$

For sufficiently small time step, the projection operator of the Monte Carlo Hamiltonian in Eq. (7) can be factorized into one-body and two-body parts by Suzuki-Trotter decomposition^{29,30}

$$e^{-\Delta\tau \hat{H}_{mc}} = e^{-\Delta\tau \hat{T}/2} e^{-\Delta\tau \frac{1}{2} \sum_{\gamma} \hat{L}_{\gamma}^2} e^{-\Delta\tau \hat{T}/2} e^{-\Delta\tau C} + \mathcal{O}(\Delta\tau^3). \quad (24)$$

The two-body propagators can be decomposed into one-body propagators by Hubbard-Stratonovich transformation³¹

$$e^{-\Delta\tau \hat{O}_1^2/2} = \int dx \frac{1}{\sqrt{2\pi}} e^{-x^2/2} e^{x\sqrt{-\Delta\tau} \hat{O}_1}, \quad (25)$$

where \hat{O}_1 represents a one-body operator and x is an auxiliary field. The projection operator becomes the integration of one-body operators in a high-dimensional auxiliary-field space

$$e^{-\Delta\tau \hat{H}_{mc}} = \int \prod_{\gamma} \left(dx_{\gamma} \frac{1}{\sqrt{2\pi}} e^{-x_{\gamma}^2/2} \right) e^{-\Delta\tau \hat{T}/2} e^{\sum_{\gamma} x_{\gamma} \sqrt{-\Delta\tau} \hat{L}_{\gamma}} e^{-\Delta\tau \hat{T}/2} e^{-\Delta\tau C} + \mathcal{O}(\Delta\tau^2). \quad (26)$$

Note that the Trotter error increase to $\mathcal{O}(\Delta\tau^2)$ during the process of grouping \hat{L}_{γ} operators. The final expression of the projection operator is

$$e^{-\Delta\tau \hat{H}_{mc}} = \int d\mathbf{x} p(\mathbf{x}) \hat{B}(\mathbf{x}), \quad (27)$$

where $\mathbf{x} = \{x_1, x_2, \dots, x_{\Gamma}\}$ denotes the auxiliary-field variables at a given time slice, $p(\mathbf{x})$ is the probability function

$$p(\mathbf{x}) = \prod_{\gamma} \frac{1}{\sqrt{2\pi}} e^{-x_{\gamma}^2/2}, \quad (28)$$

and $\hat{B}(\mathbf{x})$ is the combination of all one-body operators

$$\hat{B}(\mathbf{x}) = e^{-\Delta\tau\hat{T}/2} e^{\sum_{\gamma} x_{\gamma} \sqrt{-\Delta\tau} \hat{L}_{\gamma}} e^{-\Delta\tau\hat{T}/2} + \mathcal{O}(\Delta\tau^2). \quad (29)$$

The original projector is mapped into a high-dimensional integral of auxiliary-fields over one-body propagators, which can be evaluated by Monte Carlo techniques.

As we can see, the two-body propagator $e^{-\Delta\tau\frac{1}{2}\sum_{\gamma}\hat{L}_{\gamma}^2}$ is the one that generates the high-dimensional integral and it is more computational expensive than the one-body term $e^{-\Delta\tau\hat{T}/2}$. The algorithm will be more efficient if the magnitude of the two-body term is reduced. We can change the Monte Carlo Hamiltonian with a background subtraction trick^{16,32},

$$\hat{H}_{\text{mc}} = \hat{T} + \sum_{\gamma}^{\Gamma} \langle \hat{L}_{\gamma} \rangle \hat{L}_{\gamma} + \frac{1}{2} \sum_{\gamma}^{\Gamma} \left(\hat{L}_{\gamma} - \langle \hat{L}_{\gamma} \rangle \right)^2 + C - \frac{1}{2} \sum_{\gamma}^{\Gamma} \langle \hat{L}_{\gamma} \rangle^2, \quad (30)$$

which is still a Monte Carlo Hamiltonian with

$$\begin{aligned} \hat{T} &\leftarrow \hat{T} + \sum_{\gamma}^{\Gamma} \langle \hat{L}_{\gamma} \rangle, \\ \hat{L}_{\gamma} &\leftarrow \hat{L}_{\gamma} - \langle \hat{L}_{\gamma} \rangle, \\ C &\leftarrow C - \frac{1}{2} \sum_{\gamma}^{\Gamma} \langle \hat{L}_{\gamma} \rangle^2. \end{aligned}$$

The background subtraction applies to both electronic and lattice Hamiltonians, i.e., regardless of the details of the interaction or the form of the Hubbard-Stratonovich transformation.

C. Sampling

Monte Carlo technique is one of the most efficient methods to calculate the high-dimensional integration. Early formulation of auxiliary-field-based methods^{6,33-37} was based on the Metropolis algorithm, which is highly effective when there is no sign/phase problems (however care should be taken in handling an infinite variance problem³⁷). In the presence of the sign/phase problem, which is the case with all quantum chemical systems and all realistic materials computations, the reformulation of the framework into an open-ended random walk¹⁵ was essential. The open-ended random walk removes an ergodicity problem in the path-integral formulation which renders the sampling of positive paths exponentially-costly in at low-temperatures^{10,15}. Moreover, it provides a conceptual framework^{7,38} closely aligned with standard DFT machinery, which allowed successful and general application to electronic structure.

1. Free Projection

We initialize the $|\Psi_I\rangle$ to a Slater determinant, which is usually the Hartree-Fock (HF) solution $|\psi_{\text{HF}}\rangle$. The initial many-body wave function can be thought of as a summation of Slater determinants (so-called walkers)

$$|\Psi_I\rangle = \sum_k w_k^{(0)} |\psi_k^{(0)}\rangle, \quad (31)$$

where $w_k^{(0)} = 1$ and $|\psi_k^{(0)}\rangle = |\psi_{\text{HF}}\rangle$. The number of walkers is usually between a few hundreds to a few thousands, but can be tuned according to the computing platform to maximize efficiency for improving statistics. The projection is applied to the initial state as shown in Eq. (23), and the overall wave function after n steps can be schematically represented as

$$|\Psi^{(n)}\rangle = \sum_k w_k^{(n)} |\psi_k^{(n)}\rangle. \quad (32)$$

The weight $w_k^{(n)}$ contains products of numbers accumulated during the projection, which can be a complex number, and $|\psi_k^{(n)}\rangle$ is still a Slater determinant. The projection to the next step is carried out by

$$|\Psi^{(n+1)}\rangle = e^{-\Delta\tau\hat{H}_{mc}} |\Psi^{(n)}\rangle. \quad (33)$$

Using Eq. (27), we obtain the auxiliary field \mathbf{x}_k by sampling $p(\mathbf{x}_k)$ and applying the one-body operator to the walker k ,

$$|\psi_k^{(n+1)}\rangle = \hat{B}(\mathbf{x}_k) |\psi_k^{(n)}\rangle. \quad (34)$$

Note that the new walker remains a Slater determinant due to the Thouless theorem^{39,40}. All the numbers during the projection are absorbed into $w_k^{(n)}$ to produce the new $w_k^{(n+1)}$. To keep the walker numerically stable during the propagation, the modified Gram-Schmidt procedure is applied to each walker, and the normalization factor during the stabilization is absorbed into $w_k^{(n+1)}$. As the imaginary time step increases, some walkers will contribute significantly more than other walkers. A population control procedure is needed to replicate the walkers with larger weights and eliminate the walkers with smaller weights. There are different ways to choose the weights; for example, the weights in the algorithm without any importance sampling (free propagation) can be chosen as⁴¹

$$W_k^{(n)} = \sqrt{|w_k^{(n)}|^2 \langle \psi_k^{(n)} | \psi_k^{(n)} \rangle}. \quad (35)$$

2. Importance Sampling

We introduced the open-ended random walk procedure in the previous subsection, where the auxiliary fields are sampled by the function $p(\mathbf{x}_k)$. To further reduce the variance in the quantum Monte Carlo, we need to use importance sampling^{7,15,16}. The method requires a best guess of the ground state wave function, which is called trial wave function, $|\Psi_T\rangle$. The trial wave function can be a HF or DFT solution, a multi-determinant wave function^{41,42}, or a BardeenCooperSchrieffer (BCS) wave function^{17,43,44}. The idea of the importance sampling transformation is to guide the random walks (the sampling of the auxiliary-fields and hence the resulting determinants) during the propagation towards regions with larger overlap with the trial wave function. The weights in population control with importance sampling are given by

$$W_k^{(n)} = w_k^{(n)} \langle \Psi_T | \psi_k^{(n)} \rangle. \quad (36)$$

Note that $W_k^{(n)}$ can be a negative or complex number. When the constrained path or phaseless approximation is applied, $W_k^{(n)}$ is always positive or zero.

For sampling the auxiliary field, we change the probability density function from the product of Gaussians $p(\mathbf{x}_k)$ to a function that builds in the knowledge of $|\Psi_T\rangle$. The Hubbard-Stratonovich transformation in Eq. (25) can be rewritten as

$$\begin{aligned} e^{-\Delta\tau\hat{O}_1^2/2} &= \int dx \frac{1}{\sqrt{2\pi}} e^{-x^2/2} e^{x\sqrt{-\Delta\tau}\hat{O}_1} \\ &= \int dx \frac{1}{\sqrt{2\pi}} e^{-x^2/2} e^{x\sqrt{-\Delta\tau}\langle\hat{O}_1\rangle} e^{x\sqrt{-\Delta\tau}(\hat{O}_1 - \langle\hat{O}_1\rangle)}, \end{aligned} \quad (37)$$

where $\langle\hat{O}_1\rangle$ is the mixed estimator of \hat{O}_1 defined for a particular walker

$$\langle\hat{O}_1\rangle = \frac{\langle \Psi_T | \hat{O}_1 | \psi_k^{(n)} \rangle}{\langle \Psi_T | \psi_k^{(n)} \rangle}. \quad (38)$$

Let us define the dynamic force as $F \equiv \sqrt{-\Delta\tau}\langle\hat{O}_1\rangle$. Then Eq. (37) can be written as

$$\begin{aligned} e^{-\Delta\tau\hat{O}_1^2/2} &= \int dx \frac{1}{\sqrt{2\pi}} e^{-x^2/2} e^{xF} e^{x(\sqrt{-\Delta\tau}\hat{O}_1 - F)} \\ &= \int dx \frac{1}{\sqrt{2\pi}} e^{-x^2/2} e^{xF} \left[1 + x \left(\sqrt{-\Delta\tau}\hat{O}_1 - F \right) + \mathcal{O}(\Delta\tau) \right]. \end{aligned} \quad (39)$$

To favor the sampling of walkers with more expected contributions to the ground state, we

wish to build in the knowledge of the overlap between the trial wave function and the walker

$$\frac{\langle \Psi_T | e^{-\Delta\tau \hat{O}_1^2/2} | \psi_k^{(n)} \rangle}{\langle \Psi_T | \psi_k^{(n)} \rangle} = \int dx \frac{1}{\sqrt{2\pi}} e^{-x^2/2} e^{xF} + \mathcal{O}(\Delta\tau) \quad (40)$$

$$= \int dx \frac{1}{\sqrt{2\pi}} e^{-(x-F)^2/2} e^{F^2/2} + \mathcal{O}(\Delta\tau) . \quad (41)$$

It is clear that the most efficient way (up to the order of $\Delta\tau$) to generate the auxiliary fields is by sampling the modified probability function

$$p_I(x) = \frac{1}{\sqrt{2\pi}} e^{-(x-F)^2/2} . \quad (42)$$

With the modified probability density function, the Hubbard-Stratonovich transformation can be written as

$$e^{-\Delta\tau \hat{A}^2/2} = \int dx \frac{1}{\sqrt{2\pi}} e^{-(x-F)^2/2} e^{\frac{1}{2}F^2 - xF} e^{x\sqrt{-\Delta\tau}\hat{A}} , \quad (43)$$

$$= \int dx p_I(x) N_I(x) e^{x\sqrt{-\Delta\tau}\hat{A}} , \quad (44)$$

with $N_I(x) = e^{\frac{1}{2}F^2 - xF}$. Combining the different auxiliary-field components, we can again write the projection operator into a high dimensional integral,

$$e^{-\Delta\tau \hat{H}_{mc}} = \int d\mathbf{x} p_I(\mathbf{x}) \hat{B}_I(\mathbf{x}), \quad (45)$$

where $p_I(\mathbf{x})$ is the force-bias-shifted probability density function

$$p_I(\mathbf{x}) = \prod_{\gamma} p_I(x_{\gamma}) . \quad (46)$$

By sampling the new probability function $p_I(\mathbf{x})$, we apply the projection operator to each walker

$$w_k^{(n+1)} |\psi_k^{(n+1)}\rangle = \hat{B}_I(\mathbf{x}_{\mathbf{k}}) w_k^{(n)} |\psi_k^{(n)}\rangle . \quad (47)$$

Note that the normalization factor $N_I(x)$ in $\hat{B}_I(\mathbf{x}_{\mathbf{k}})$ will be absorbed into $w_k^{(n)}$ and the operators in $\hat{B}_I(\mathbf{x}_{\mathbf{k}})$ will be applied to $|\psi_k^{(n)}\rangle$ during the propagation.

The importance sampling uses the knowledge of the trial wave function $|\Psi_T\rangle$ to reduce the Monte Carlo fluctuation. In the above we have presented it as a reformulation of the Hubbard-Stratonovich transformation. Importance sampling in the usual sense does not change the expectation value, only the variance. When there is a sign problem, this holds in that the computed energy is always the constrained-path result with the same trial wave

function, whether importance sampling is applied or not. When there is a phase problem, however, we are using the “importance-sampling” transformation in *an unconventional sense*, to select a unique gauge choice. In this case, the phaseless approximation is defined with respect to the trial wave function *after* importance sampling; the similarity transformation is essential and affects the expectation value as well as the variance⁷.

3. *Constrained Path and Phaseless Approximations*

We address the sign and phase problem in this subsection, which stems from the fact that a Slater determinant, $|\psi_k\rangle$, remains invariant to arbitrary rotations, such as $e^{i\theta}|\psi_k\rangle$. During the propagation, the walkers will have random contributions to the phase accumulated from the propagator $\hat{B}(\mathbf{x})$, which contains stochastically sampled auxiliary-fields and complex matrix elements. These phases will eventually cause the random walkers to populate the entire complex plane and the statistical average of the walkers, in the sense of Eq. (32), will approach zero, which leads to an decay in observable signal-to-noise ratios. Unless the development of the phase (or sign) is prevented explicitly by symmetry, this decay will occur, and its onset is exponential with projection time or inverse temperature⁴⁵. The loss of signal manifests itself as infinite variance in the Monte Carlo estimators. (Note that the reverse is not true: an infinite variance problem can appear in a large number of sign-problem-free AFQMC calculations, requiring care to mitigate³⁷.)

When the propagators $\hat{B}(\mathbf{x})$ are real, the only possible phases in a walker are 0 and π . This is the commonly referred to sign problem, which occurs widely in lattice model calculations. We impose a constrained path approximation^{15,38} by requiring that all walkers maintain a positive overlap with the trial wave function during the propagation

$$W_k^{(n)} > 0, \tag{48}$$

where $W_k^{(n)}$ is defined in Eq. (36). It can be shown that the constraint will be exact if the trial wave function is the ground state wave function. However, the ground state wave function is usually unknown, and the use of $|\Psi_T\rangle$ in implementing the constraint will result in a small bias^{46,47}.

The phaseless approximation^{7,38} is employed to control the phase problem when the propagators are complex. It defines a unique gauge θ with respect to the knowledge of the

true ground state, by projecting a complex walker onto the positive real axis

$$W_k^{(n)} \rightarrow \text{Re} \left[W_k^{(n)} \right] \times \max(0, \cos(\Delta\theta)), \quad (49)$$

where the phase angle $\Delta\theta$ for each component of the auxiliary-field x is

$$\Delta\theta = \arg \left[\frac{\langle \Psi_T | \hat{B}(x) | \psi_k^{(n)} \rangle}{\langle \Psi_T | \psi_k^{(n)} \rangle} \right] \approx \mathcal{O}(\text{Im}(xF)). \quad (50)$$

The cosine projection will ensure that the density of the walkers vanish at the origin of the complex plane of $\langle \Psi_0 | \psi \rangle$ (or of the proxy $\langle \Psi_T | \psi \rangle$ when implemented as a phaseless approximation using Ψ_T). Note that phaseless approximation is smoothly connected to the constrained path approximation, since $\Delta\theta$ is zero if $\hat{B}(\mathbf{x})$ is real¹⁶.

D. Measurement

After the imaginary-time projection is converged within the expected statistical accuracy, we can measure the ground-state properties with additional projection time steps. For a physical quantity \hat{A} that commutes with the Hamiltonian, $[\hat{A}, \hat{H}] = 0$, we use the mixed estimator

$$\begin{aligned} \langle \hat{A} \rangle_{mix} &= \frac{\langle \Psi_T | \hat{A} | \Psi^{(n)} \rangle}{\langle \Psi_T | \Psi^{(n)} \rangle} \\ &= \frac{\sum_k w_k^{(n)} \langle \Psi_T | \hat{A} | \psi_k^{(n)} \rangle}{\sum_k w_k^{(n)} \langle \Psi_T | \psi_k^{(n)} \rangle}. \end{aligned} \quad (51)$$

It is common to introduce the ‘‘local’’ measurement:

$$A_L[\Psi_T, \Phi] \equiv \frac{\langle \Psi_T | \hat{A} | \Phi \rangle}{\langle \Psi_T | \Phi \rangle}, \quad (52)$$

so that Eq. (51) can be easily calculated by

$$\langle \hat{A} \rangle_{mix} = \frac{\sum_k W_k^{(n)} A_L[\Psi_T, \psi_k^{(n)}]}{\sum_k W_k^{(n)}}. \quad (53)$$

Note that $W_k^{(n)}$ is the weight in Eq. (36), used in the population control following importance sampling transformation, both in the constrained path and phaseless formulations.

If \hat{A} does not commute with \hat{H} , the mixed estimator is biased. The back-propagation technique^{15,48,49} was proposed to remove this bias, which measures the physical quantity by

$$\langle \hat{A} \rangle_{bp} = \frac{\sum_k w_k^{(n)} \langle \Psi_T | e^{-m\Delta\tau \hat{H}_{mc}} \hat{A} | \psi_k^{(n)} \rangle}{\sum_k w_k^{(n)} \langle \Psi_T | e^{-m\Delta\tau \hat{H}_{mc}} | \psi_k^{(n)} \rangle}. \quad (54)$$

In the framework of open-ended random walkers, the back-propagation can be represented by

$$\langle \hat{A} \rangle_{bp} = \frac{\sum_k w_k^{(n+m)} \langle \Psi_T | \hat{B}(\mathbf{x}_{n+m}) \cdots \hat{B}(\mathbf{x}_{n+1}) \hat{A} | \psi_k^{(n)} \rangle}{\sum_k w_k^{(n+m)} \langle \Psi_T | \psi_k^{(n+m)} \rangle} \quad (55)$$

$$= \frac{\sum_k W_k^{(n+m)} A_L[\phi_m, \Psi_k^{(n)}]}{\sum_k W_k^{(n+m)}}, \quad (56)$$

where the ϕ_m in the local measurement A_L is the back-propagated Slater determinant

$$|\phi_m\rangle = \hat{B}^\dagger(\mathbf{x}_{n+1}) \cdots \hat{B}^\dagger(\mathbf{x}_{n+m}) |\Psi_T\rangle. \quad (57)$$

This formalism is exact and by-passes the difficulty of a brute-force estimator of matching two independent populations for the bra and ket⁴⁸. In practice, the constrained path (phaseless) approximation breaks the symmetry in the imaginary time axis. The back-propagated wave function is not equal to $|\Psi_0^{CP}\rangle$ (or $|\Psi_0^{PL}\rangle$ in phaseless). This causes a bias which is typically larger than that of a pure estimator formed by two $|\Psi_0^{CP}\rangle$'s ($|\Psi_0^{PL}\rangle$'s). In phaseless calculations, an additional improvement is achieved⁴⁹ if we restore the phases to the weight $W_k^{(n+m)}$ (for the back-propagation portion only) in Eq. (56),

$$W_k^{(n+m)} = W_k^{(n+m)} \prod_{w=n+1}^{n+m} \frac{1}{\max[0, \cos(\Delta\theta_k^{(w)})]}. \quad (58)$$

Note that the back-propagation step m needs to be large enough to reach the convergence of $|\phi_m\rangle$ while keeping the accumulated phase stable.

III. ADVANCED IMPLEMENTATION

The AFQMC algorithm as outlined above can be implemented by linear algebra operations for general basis sets. The scaling of the algorithm is M^4 in the naive implementation, with large prefactors. We discuss an advanced implementation in this section, which reduces the scaling to $M^2 N^2$ in the measurement. To facilitate the discussion, we sketch a summary of the AFQMC algorithm:

1. Set up the initial state $|\Psi_I\rangle = \sum_k w_k |\psi_k\rangle$. For example we can choose $w_k = 1$ and $|\psi_k\rangle$ as $|\Psi_T\rangle$. (A multi-determinant $|\Psi_T\rangle$ can be sampled according to the squared absolute value of the coefficients.)

2. Compute the overlap $\langle \Psi_T | \psi_k \rangle$ and apply the constrained path or phaseslss approximation to the weight. The walker is killed by setting the weight to zero.
3. If the weight is non-zero, compute the dynamic force components $\{F_\gamma\}$.
4. Sample the auxiliary field \mathbf{x} from the modified probability function involving the force bias components $F_\gamma, p_I(\mathbf{x})$ in Eq (46). Calculate the phase $\Delta\theta_k$ for cos projection.
5. Propagate the walker with $\hat{B}_I(\mathbf{x})$, and update the weight w_k according to the normalization (Eq (47)).
6. Repeat steps 2 to 5 for all walkers, which forms one step of the projection.
7. Periodically perform population control procedure to adjust the weights $\{W_k\}$.
8. Periodically perform the modified Gram-Schmidt procedure to orthonormalize the orbitals of the walkers.
9. Periodically measure the ground state properties after a sufficiently large imaginary time of initial equilibration.

There are three main computational components;

- Calculate the weight: $W_k = w_k \langle \Psi_T | \psi_k \rangle$
- Calculate the force bias: $F_\gamma = \sqrt{-\Delta\tau} \langle \Psi_T | \hat{L}_\gamma | \psi_k \rangle / \langle \Psi_T | \psi_k \rangle$.
- Compute the local observable in measurements $\langle \hat{A} \rangle = \langle \Psi_T | \hat{A} | \psi_k \rangle / \langle \Psi_T | \psi_k \rangle$.

Below we separately discuss the details of how to speed up the calculations when the trial wave function is a *single-determinant* and when it is a *multi-determinant* in the form of the complete active-space self-consistent field (CASSCF).

A. Single-determinant

For a single-determinant trial wave function, we assume its matrix representation is $(\Psi_T^\uparrow, \Psi_T^\downarrow)$, where Ψ_T^σ is a $M \times N^\sigma$ matrix and N^σ is the number of particles for spin σ . The walkers in AFQMC are also single-determinants, each with the matrix representation $(\psi_k^\uparrow, \psi_k^\downarrow)$.

1. Weight

The weight $W_k = w_k \langle \Psi_T | \psi_k \rangle$ is calculated from the overlap between the trial wave function and each walker. In the matrix representation, the overlap is a determinant

$$\langle \Psi_T | \psi_k \rangle = \det \left(\Psi_T^{\uparrow \dagger} \psi_k^{\uparrow} \right) \det \left(\Psi_T^{\downarrow \dagger} \psi_k^{\downarrow} \right). \quad (59)$$

The computation of the overlap, with the scaling of $MN^{\sigma^2} + N^{\sigma^3}$, is generally small compared to other operations. We save the LU decomposition of the matrix $\Psi_T^{\sigma \dagger} \psi_k^{\sigma}$ when computing the overlap and determinant, which will be useful for calculating $\left(\Psi_T^{\sigma \dagger} \psi_k^{\sigma} \right)^{-1}$ and the Green's function in the following discussion.

2. Force bias

The force bias is the measurement of the one-body operator \hat{L}_γ . To measure any one-body operator, we first introduce the one-particle reduced density matrix

$$G_{ij}^\sigma = \frac{\langle \Psi_T | a_i^\dagger a_j | \psi_k \rangle}{\langle \Psi_T | \psi_k \rangle} \quad (60)$$

$$= \left[\psi_k^\sigma \left(\Psi_T^{\sigma \dagger} \psi_k^\sigma \right)^{-1} \Psi_T^{\sigma \dagger} \right]_{ji}. \quad (61)$$

If the matrix representation of \hat{L}_γ is L_γ^σ , the measurement of force is given by

$$F_\gamma = \sqrt{-\Delta\tau} \sum_{ij} \sum_{\sigma} (L_\gamma^\sigma)_{ij} G_{ij}^\sigma \quad (62)$$

$$= \sqrt{-\Delta\tau} \sum_{\sigma} \text{Tr} \left[L_\gamma^\sigma \psi_k^\sigma \left(\Psi_T^{\sigma \dagger} \psi_k^\sigma \right)^{-1} \Psi_T^{\sigma \dagger} \right] \quad (63)$$

$$= \sqrt{-\Delta\tau} \sum_{\sigma} \text{Tr} \left[\left(\Psi_T^{\sigma \dagger} L_\gamma^\sigma \right) \Theta_k^\sigma \right], \quad (64)$$

where $\Theta_k^\sigma = \psi_k^\sigma \left(\Psi_T^{\sigma \dagger} \psi_k^\sigma \right)^{-1}$. Since $\Psi_T^{\sigma \dagger} L_\gamma^\sigma$ is independent of walkers during the propagation, we can pre-compute it and use the stored results throughout the whole AFQMC simulation. Θ_k^σ is calculated by solving a linear equation with LU decomposition of $\Psi_T^{\sigma \dagger} \psi_k^\sigma$ saved before. Θ_k^σ can be saved for the measurements of other quantities. With the procedures above, the calculation of the force bias only scales as $\Gamma MN^\sigma + MN^{\sigma^2}$.

3. Measurements

For the measurement of any one-body operator, we use the same trick as in the calculation of the force bias. The most costly part in the measurement is the full Coulomb interaction energy

$$\hat{V} = \frac{1}{2} \sum_{\gamma}^{\Gamma} \sum_{ijkl}^M \sum_{\sigma\rho} L_{(il)\gamma} L_{(kj)\gamma}^* \frac{\langle \Psi_T | a_{i\sigma}^{\dagger} a_{j\rho}^{\dagger} a_{k\rho} a_{l\sigma} | \psi_k \rangle}{\langle \Psi_T | \psi_k \rangle}. \quad (65)$$

With the generalized Wicks theorem^{50,51}, we have

$$\frac{\langle \Psi_T | a_{i\sigma}^{\dagger} a_{j\rho}^{\dagger} a_{k\rho} a_{l\sigma} | \psi_k \rangle}{\langle \Psi_T | \psi_k \rangle} = G_{il}^{\sigma} G_{jk}^{\rho} - \delta_{\sigma\rho} G_{ik}^{\sigma} G_{jl}^{\sigma}, \quad (66)$$

The interaction energy can be calculated as

$$\hat{V} = \frac{1}{2} \sum_{\gamma}^{\Gamma} \sum_{ijkl}^M \sum_{\sigma\rho} L_{(il)\gamma} L_{(kj)\gamma}^* (G_{il}^{\sigma} G_{jk}^{\rho} - \delta_{\sigma\rho} G_{ik}^{\sigma} G_{jl}^{\sigma}) \quad (67)$$

$$= \frac{1}{2} \sum_{\gamma}^{\Gamma} \left[\left(\frac{\langle \Psi_T | \hat{L}_{\gamma} | \psi_k \rangle}{\langle \Psi_T | \psi_k \rangle} \right)^2 - \sum_{\sigma} \text{Tr} \left(\Psi_T^{\sigma\dagger} L_{\gamma}^{\sigma} \Theta_k^{\sigma} \Psi_T^{\sigma\dagger} L_{\gamma}^{\sigma} \Theta_k^{\sigma} \right) \right], \quad (68)$$

where the first part (Hartree term) is just the square of the force. To handle the second part (exchange term), which is more costly, we order the matrix operations as

$$\left[\left(\Psi_T^{\sigma\dagger} L_{\gamma}^{\sigma} \right) \Theta_k^{\sigma} \right] \left[\left(\Psi_T^{\sigma\dagger} L_{\gamma}^{\sigma} \right) \Theta_k^{\sigma} \right], \quad (69)$$

which scales as $\Gamma M N^{\sigma^2}$. Recent progress has been able to reduce the scaling by introducing different forms of low-rank decomposition^{28,52,53}. We will not discuss the implementation of these approaches here, although they do not require fundamentally different computational ingredients beyond what we have covered.

B. Multi-determinant

For a general multi-determinant trial wave function, we can apply the procedure discussed above for each determinant. This implementation will cause an additional scaling factor N_d , which is the number of determinants in the trial wave function. In the limit of large N_d , it becomes inefficient in both computational time and memory requirements. One of the most widely used trial wave functions is the CASSCF wave function, where all the determinants are built from the some canonical orbitals. It is natural to take advantage of the properties of

the CASSCF wave function to reduce computational scaling, similar to how fast updates of one or a few components of the auxiliary-fields were handled via Sherman-Morrison formula. An implementation of the CASSCF trial wave function speedup was presented in Ref.²⁶. Here we present the details of our implementation which reduces the scaling to sub-linear in N_d .

The CASSCF wave function has the form

$$|\Psi_T\rangle = \sum_{m=1}^{N_d} c_m |\phi_m\rangle, \quad (70)$$

where the coefficient c_m is a c-number and $|\phi_m\rangle$ is a Slater determinant with the matrix representation $(\phi_m^\uparrow, \phi_m^\downarrow)$. As mentioned before, pairs of these Slater determinants can share some columns with each other. It is also possible that the matrix for one spin component is identical in two determinants, for example, $\phi_m^\uparrow = \phi_n^\uparrow$, while $\phi_m^\downarrow \neq \phi_n^\downarrow$.

We define the group $\varphi^\sigma = (\phi_1^\sigma, \phi_2^\sigma, \dots, \phi_{S_d^\sigma}^\sigma)$, which removes duplicate Slater determinants, with S_d^σ specifying the number of unique spin- σ determinants. By the mapping from ϕ^σ to φ^σ , the CASSCF wave function becomes

$$|\Psi_T\rangle = \sum_{m=1}^{N_d} c_m |\varphi_{m_\uparrow}^\uparrow, \varphi_{m_\downarrow}^\downarrow\rangle. \quad (71)$$

Here, each m is mapped to the index $(m_\uparrow, m_\downarrow)$ in the non-repetitive group φ . In the following, we only deal with φ , which reduces the number of operations from N_d to $S_d^\uparrow + S_d^\downarrow$. Note that $S_d^\sigma \propto \sqrt{N_d}$ for the spin-balanced systems.

To use the common orbitals φ , we define a tree structure that minimizes the distance between two Slater determinants, where “distance” means the number of different orbitals between the two Slater determinants. An example of the tree structure for 10 Slater determinants is shown in Fig. 1.

We define the first parent of the tree structure, which is the determinant with the largest $|c_m|^2$. In Fig. (1), the first parent is φ_1^σ in the filled red circle. Then we calculate the distance between the first parent-determinant and all other determinants, and choose its child-determinants with the shortest distances. In the figure φ_2^σ , φ_4^σ , and φ_8^σ are child-determinants, since they have the shortest distance $d = 1$. The second parent is chosen among them. We calculate the distances between each candidate and the rest of the determinants. The one with the shortest distance is selected as the next parent-determinant. If two candidates have the same shortest distance, the one with more child-determinants is

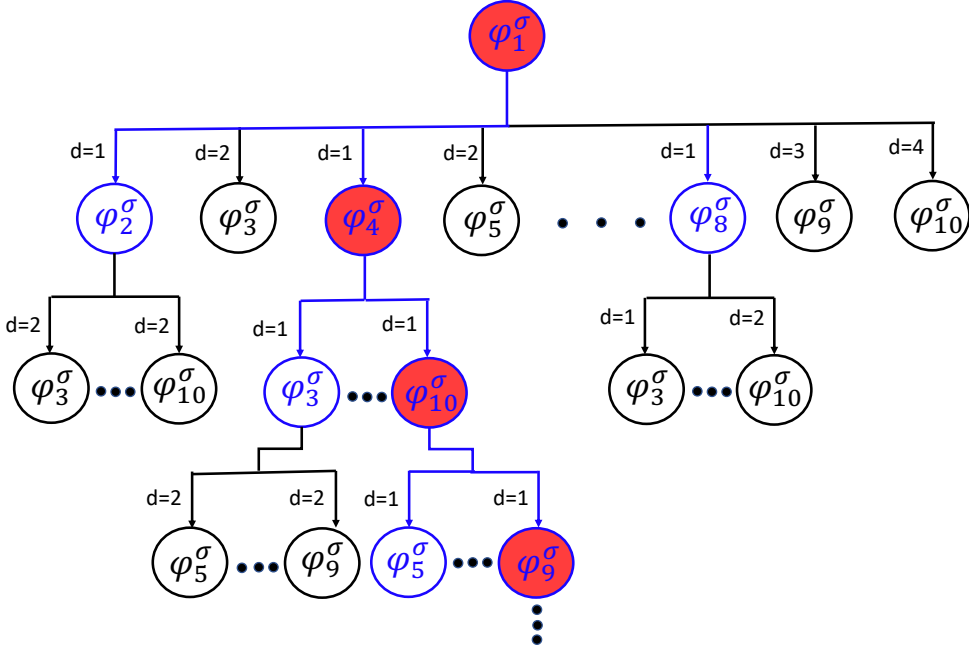


FIG. 1. A tree structure of the common orbitals φ , for 10 Slater determinants. The parent-determinants are filled red circle and the corresponding immediate child-determinants are connected by blue lines. The distances between a parent determinant and all descendants are labelled as d , by the side of the arrows. The tree structure finds a good sequence of 10 Slater determinants, which is connected by the blue lines.

selected as the next parent-determinant. For example, φ_2^σ cannot be a parent determinant since its shortest distance ($d = 2$) is larger than that of φ_4^σ and φ_8^σ ($d = 1$). As φ_4^σ has two child determinants ($\varphi_3^\sigma, \varphi_{10}^\sigma$) with $d = 1$, while φ_8^σ has one child-determinant (φ_3^σ) with $d = 1$, φ_4^σ is preferred as a parent determinant. The same procedure is applied to find the next parent-determinant, until all Slater determinants are on the tree structure.

With the tree structure established, we will only do a full computation for the first parent-determinant. The ShermanMorrison formula is then used to achieve fast updates for the child-determinants. For the example in Fig. 1, the order during our simulation is:

1. Full calculation on φ_1^σ .
2. Use the information on φ_1^σ to calculate $\varphi_2^\sigma, \varphi_4^\sigma, \varphi_8^\sigma$.
3. Use the information on φ_4^σ to calculate $\varphi_3^\sigma, \varphi_{10}^\sigma$.

4. Use the information on φ_{10}^σ to calculate $\varphi_5^\sigma, \varphi_9^\sigma$.
5. ...

1. Weight

The weight with a multi-determinant trial wave function is given by

$$W_k = w_k \langle \Psi_T | \psi_k \rangle \quad (72)$$

$$= w_k \sum_{m=1}^{N_d} c_m^* \det \left[(\varphi_{m\uparrow}^\dagger)^\dagger \psi_k^\uparrow \right] \det \left[(\varphi_{m\downarrow}^\dagger)^\dagger \psi_k^\downarrow \right]. \quad (73)$$

We next consider the computation of the overlap matrix $\varphi_{m\sigma}^{\sigma\dagger} \Psi_k^\sigma$. We define a Φ_F^σ matrix that contains all columns in $\varphi_{m\sigma}^\sigma$. The corresponding overlap matrix is

$$O_F^\sigma = \Phi_F^{\sigma\dagger} \psi_k^\sigma. \quad (74)$$

For each $\varphi_{m\sigma}^\sigma$, we select the rows in the O_F matrix to build the overlap matrix. If the overlap matrix of a parent-determinant is A_p^σ , its child-determinant A_c^σ , with a distance d_c^σ , has overlap matrix

$$A_c^\sigma = A_p^\sigma + U^\sigma V^\sigma, \quad (75)$$

where V^σ is a $d_c^\sigma \times N^\sigma$ matrix and U^σ is a $N^\sigma \times d_c^\sigma$ matrix. Note that most of the elements in U^σ are zero, with the nonzero elements residing only in the rows which are different between A_c and A_p . Using ShermanMorrison formula, we can update the determinant of A_c^σ by

$$\frac{\det A_p^\sigma}{\det A_c^\sigma} = \det \left[1 - (1 + V(A_p^\sigma)^{-1}U)^{-1}V(A_p^\sigma)^{-1}U \right]. \quad (76)$$

This is similar to the fast updates in AFQMC widely applied in lattice models; it has also been applied in diffusion MC with multi-determinant trial wave functions⁵⁴.

When the child-determinant becomes a parent-determinant, its inverse can be calculated by

$$(A_c^\sigma)^{-1} = (A_p^\sigma)^{-1} - (A_p^\sigma)^{-1}U(1 + V(A_p^\sigma)^{-1}U)^{-1}V(A_p^\sigma)^{-1}. \quad (77)$$

With $(A_p^\sigma)^{-1}$, we can quickly calculate the overlap between the trial wave function and walkers. Since $(A_p^\sigma)^{-1}$ is also updated through the tree structure, we need to periodically re-calculate the inverse from scratch to avoid numerical instability.

2. Force bias

The force bias for multi-determinant trial wave function is

$$F_\gamma = \sqrt{-\Delta\tau} \frac{\langle \Psi_T | \hat{L}_\gamma | \psi_k \rangle}{\langle \Psi_T | \psi_k \rangle} \quad (78)$$

$$= \sqrt{-\Delta\tau} \sum_\sigma \frac{\sum_{m=1}^{N_d} c_m^* \langle \varphi_{m\uparrow}^\uparrow | \psi_k^\uparrow \rangle \langle \varphi_{m\downarrow}^\downarrow | \psi_k^\downarrow \rangle \frac{\langle \varphi_{m\sigma}^\sigma | \hat{L}_\gamma^\sigma | \psi_k^\sigma \rangle}{\langle \varphi_{m\sigma}^\sigma | \psi_k^\sigma \rangle}}{\sum_{m=1}^{N_d} c_m^* \langle \varphi_{m\uparrow}^\uparrow | \psi_k^\uparrow \rangle \langle \varphi_{m\downarrow}^\downarrow | \psi_k^\downarrow \rangle}. \quad (79)$$

The calculation of $c_m^* \langle \varphi_{m\uparrow}^\uparrow | \psi_k^\uparrow \rangle \langle \varphi_{m\downarrow}^\downarrow | \psi_k^\downarrow \rangle$ has been discussed in the previous section. We focus on the local measurement

$$\frac{\langle \varphi_{m\sigma}^\sigma | \hat{L}_\gamma^\sigma | \psi_k^\sigma \rangle}{\langle \varphi_{m\sigma}^\sigma | \psi_k^\sigma \rangle} = \text{Tr} \left[(\varphi_{m\sigma}^\sigma)^\dagger L_\gamma^\sigma \Theta_k^\sigma \right], \quad (80)$$

with $\Theta_k^\sigma = \psi_k^\sigma \left[(\varphi_{m\sigma}^\sigma)^\dagger \psi_k^\sigma \right]^{-1}$. Similar to the force bias for single-determinant $|\Psi_T\rangle$, we only calculate $(\varphi_{m\sigma}^\sigma)^\dagger L_\gamma^\sigma$ once through the whole AFQMC simulation. In practice, we calculate $\Phi_F^{\sigma\dagger} L_\gamma^\sigma$ and save it to memory. $(\varphi_{m\sigma}^\sigma)^\dagger L_\gamma^\sigma$ can be constructed from $\Phi_F^{\sigma\dagger} L_\gamma^\sigma$ by selecting corresponding rows, which dramatically reduces the memory requirement. Note that Θ_k^σ can also be updated from the parent-determinant using the ShermanMorrison formula

$$\Theta_{kc}^\sigma = \Theta_{kp}^\sigma - \Theta_{kp}^\sigma U (1 + V(A_p^\sigma)^{-1} U)^{-1} V(A_p^\sigma)^{-1}, \quad (81)$$

where Θ_{kc}^σ is the targeted child-determinant and Θ_{kp}^σ is for the parent-determinant.

The computation of the interaction energy is similar to the procedure above in computing the force bias, so we omit a more detailed discussion. Using the tree structure, the additional scaling with N_d is reduced to sub-linear of N_d . A comparison between the naive implementation and the fast algorithm described here is shown in Fig. 2. A simple example is used, with multi-determinant trial wave functions from a CASSCF calculation (obtained with PyScf⁵⁵). It is clear that the advanced implementation leads to a drastic speedup. (This implementation was employed in the recent Simons benchmark project⁵⁶.)

IV. SELF-CONSISTENT AFQMC

The trial wave function is used to control the sign and phase problems in the AFQMC calculation. In the previous section, we presented the advanced implementation for multi-determinant trial wave functions, which have been shown to systematically yield AFQMC

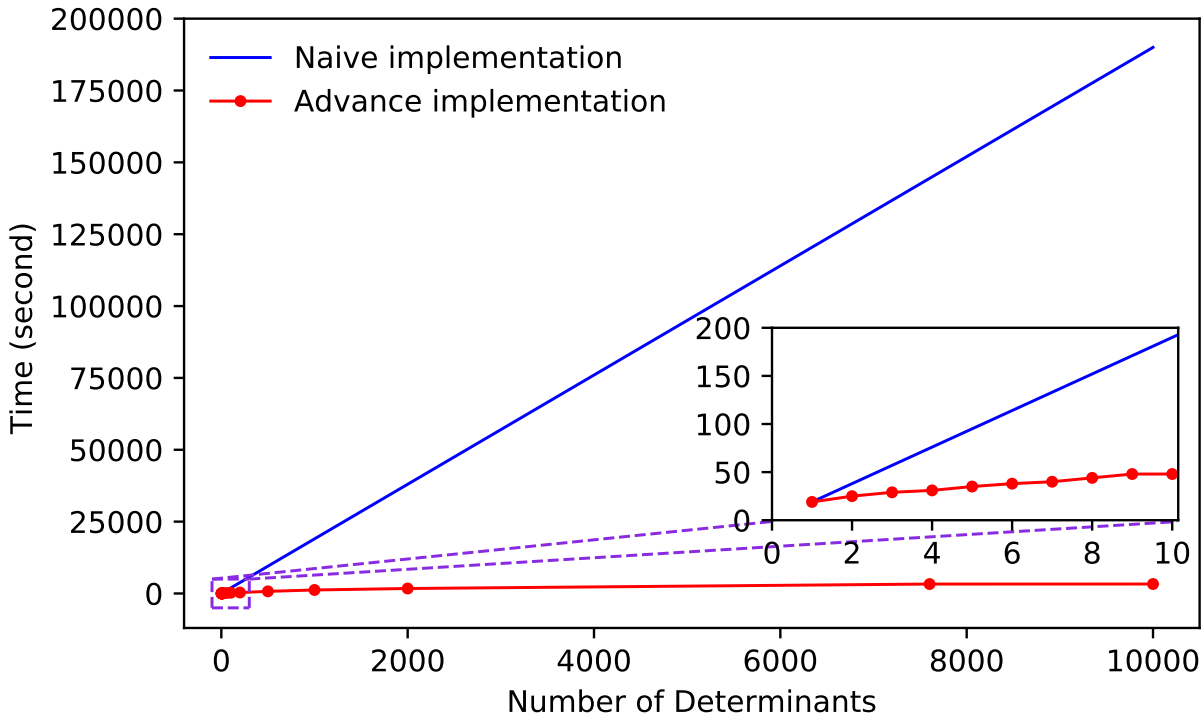


FIG. 2. The timing for AFQMC simulations with a multi-determinant trial wave function. The systems is the O atom in the ccpVdZ basis. The naive implementation scales linearly with the number of determinants in the trial wave function, which is shown by the blue extrapolated line. Timing measurements from our implementation is shown by the red dots. With 10,000 determinants, the speedup is more than $\times 60$. The inset shows a zoom of up to 10 determinants in the trial wave function.

results of chemical accuracy in a large number of molecules (e.g., Refs^{56–58}). The improved scaling of multi-determinant trial wave function to sub-linear in N_d thus provides a significant boost towards systematic and general applications in molecular systems.

In extended systems, however, the number of determinants needed in the most challenging strongly correlated materials will grow exponentially with system size in a CASSCF-like treatment. It is thus important to have size-consistent alternatives. In addition to the single-determinant trial wave function, which has been shown to be very accurate in a large variety of systems, interesting possibilities exist with GHF and symmetry-restoration⁴², BCS⁴³ and HFB¹⁷, and a stochastic representation of Jastrow factors⁵⁹. Recently a self-consistent constraint has been proposed and shown to further reduce the systematic error

from the constrained path approximation in lattice model calculations, especially in quantities such as spin and charge density and the reduced density matrix^{45,60}. Conceptually this provides a framework in which the outcome of one AFQMC calculation can be fed into the next iteration to achieve a systematically improvable self-consistent procedure.

Here we consider the generalization of the self-consistent AFQMC idea to *ab initio* computations in molecules and solids. Two flavors of the self-consistent approach have been suggested⁶⁰. The first is to couple the AFQMC calculation to an independent-electron calculation.^{45,60} The reduced one-body density matrix obtained from AFQMC is fed back to the independent-electron calculation which can be, for example, HF. The effective interaction in the HF is tuned so as to produce a density (or density matrix) which best matches the AFQMC result. The output Slater determinant wave function is then used for another AFQMC calculation. The process is iterated until the density matrix is converged. In lattice model calculations, this self-consistent procedure often involved tuning an effective U parameter. The second flavor of the self-consistent approach is to diagonalize the AFQMC density matrix and select natural orbitals up to N_σ for the trial wave function, and to iterate until the resulting natural orbitals do not change any further.

We first study the second approach, self-consistent computation from diagonalizing the density matrix, using a simple example. In Fig. 3, results are shown for the O atom using an effective-core potential (ECP, see Ref.⁵⁶ for details of the ECP), with $4 \uparrow 2 \downarrow$ electrons. The AFQMC simulation starts from a HF trial wave function. The density matrices calculated by the AFQMC simulation using this trial wave function are diagonalized for both spin species, and the resulting N^σ natural orbitals are taken to form a single Slater determinant wave function, which is then used as a trial wave function in the new AFQMC simulation. The procedure is iterated until the density matrices are converged. Interestingly, starting from a HF trial wave function, the majority-spin density matrix shown in the top panel exhibits a non-monotonic behavior, which converges after 15 iterations. We see that both the density matrix and the electronic density are improved upon convergence of the self-consistent loop.

We next generalize the first self-consistent method mentioned above to the formalism for real materials, coupling AFQMC to an effective independent-electron calculation. In particular, rather than viewing a DFT (including HF) calculation as an independent-electron method to treat the *original* Hamiltonian, we view it as a proxy calculation with an *effective* Hamiltonian whose goal is to produce a single determinant with an electronic density (or

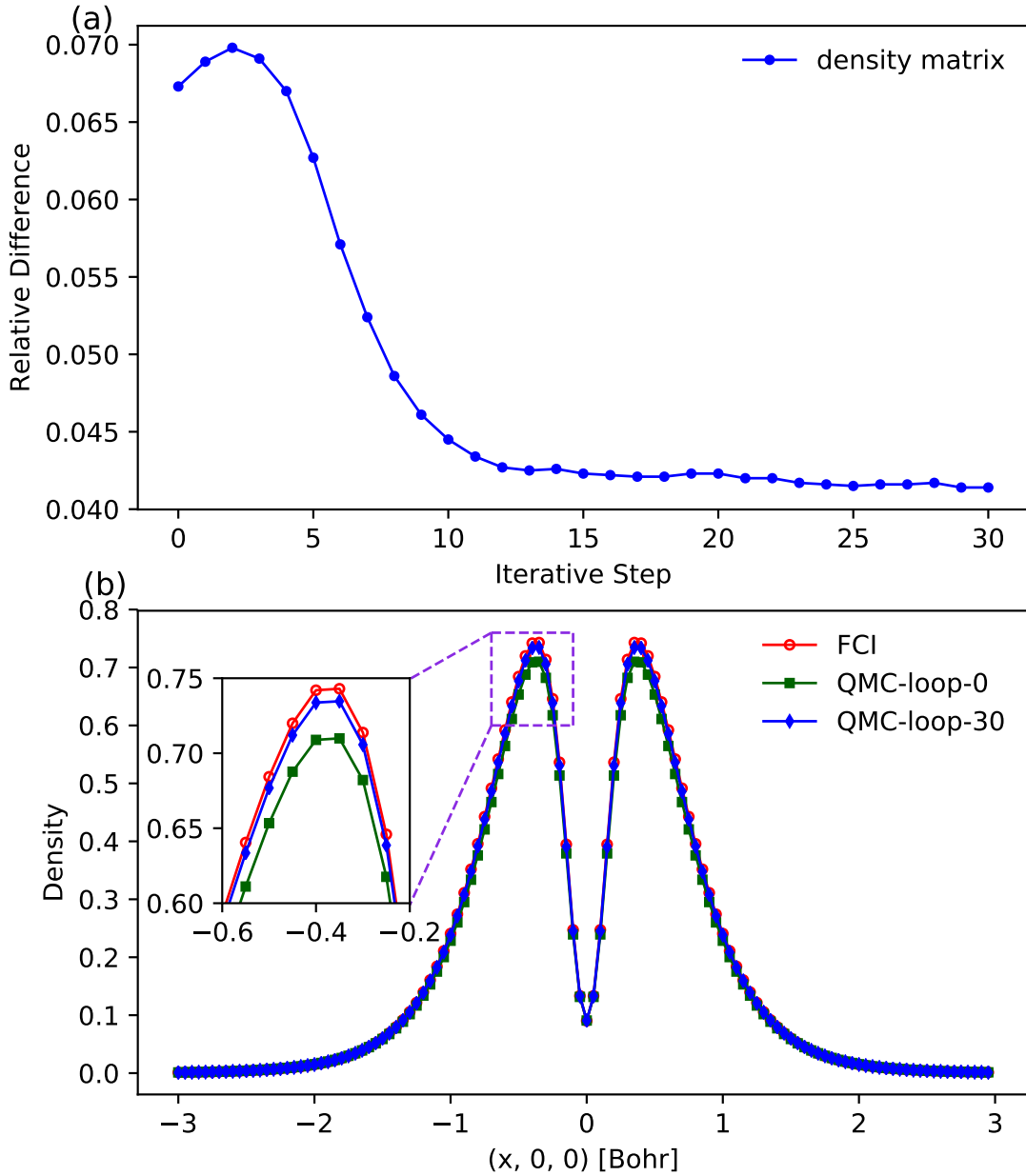


FIG. 3. Self-Consistent AFQMC calculation using the natural orbitals of the computed one-body density matrix. Results are shown for the O^+ atom in the cc-pVdZ basis, using an ECP. (a) The relative difference of one-body density matrix of the majority spin (4 electrons) computed by AFQMC with respect to FCI results, $\|G_{\text{AFQMC}} - G_{\text{FCI}}\|/\|G_{\text{FCI}}\|$, as a function of self-consistent iteration steps. (b) The computed electronic density of the majority spin on a line cut through the atom (distance x in Bohr). The density from AFQMC using the HF trial wave function (loop 0) is improved by the self-consistency upon convergence, as compared to the FCI density.

density matrix) best matching that of the AFQMC (always done with the original Hamiltonian, of course). One way to think about the effective Hamiltonian is in terms of the many different DFT functionals in existence, as well as additional ones in which the strength of the Coulomb interaction is allowed to deviate from the true electron-electron interaction. In this way, the self-consistent AFQMC procedure, in addition to being a systematically improvable many-body method via the trial wave function, can also be viewed as an automatic “screener” for density functionals.

We illustrate this approach using the BH molecule as an example. For the auxiliary independent-electron calculations, we use a form for the effective Hamiltonian closely resembling the popular B3LYP functional (as implemented in Pyscf⁵⁵):

$$E_{xc} = \beta \left[\alpha E_x^{\text{HF}} + (0.1 - 0.1\alpha) E_x^{\text{LDA}} + (0.9 - 0.9\alpha) E_x^{\text{B88}} + (1 - d) E_c^{\text{LYP}} + d E_c^{\text{VWN}} \right]. \quad (82)$$

In B3LYP, $\beta = 1.0$, $\alpha = 0.2$, and $d = 0.19$. The parameter α tunes the percentage of the exact exchange, and β scales the effective strength of the Coulomb interaction. We will allow both parameters to vary in our auxiliary independent-electron calculations. We start our self-consistent process from an initial trial wave function generated with the parameters $\alpha = 0.80$ and $\beta = 1.0$, which is way off from B3LYP or any reasonable mean-field approximation. This yields a ground-state energy which is rather accurate at step 0 but with poor AFQMC result on the one-body density matrix, as shown in Fig. 4. We then perform our auxiliary “DFT” calculations by tuning α and β with an interval 0.005, identifying the parameter choices which minimizes the difference between the DFT density matrix and that from AFQMC in the previous iteration. The resulting DFT wave function is fed into the next step AFQMC as trial wave function. This process reduces the density matrix bias (while giving non-monotonic results in the AFQMC total energy from the mixed estimator, which is not variational^{7,38}), and converges to $\alpha = 0.35$ and $\beta = 0.975$. This is far away from the initial parameter choices, and reasonably close to the B3LYP values. As seen in the top panel, the DFT density matrix result also improves with the AFQMC, and the final answer at the selected parameters is in fact better than that from B3LYP. It is worth noting that these results are for a finite basis set. DFT functionals including B3LYP are designed for the complete basis set limit, and there can be non-negligible effects in comparing them. However, this is not relevant to the point of our test, which shows that the self-consistent procedure can find an effective Hamiltonian which yields a better description of the particular

Hamiltonian.

This simple example serves as a proof-of-concept demonstration of the coupling between AFQMC and an auxiliary independent-electron calculation to achieve self-consistency, matching the density matrix (or the electronic density). Clearly the procedure can be made more general and elaborate. For example, for simplicity we did not vary the correlation part of the functional, other than the overall scale β . One could introduce many more parameters, and choose any physically motivated form of the effective Hamiltonian. The results above show that this is a very promising avenue for not only systematically improvable AFQMC calculations in real materials but also screening DFT functionals which could be used in related and larger systems, or be coupled to AFQMC for embedding⁶¹ to extend system size.

V. SUMMARY

In this article, we reported our recent progress on several fronts in continuing to develop the AFQMC method for real materials. The AFQMC method is highly accurate for a wide range of systems, as demonstrated by recent benchmark studies^{46,47,56,62,63}. It has a low-power scaling with the size of the systems and is naturally parallel on high performance computing platforms. The AFQMC method can be applied to any Hamiltonian which can be written in the MC Hamiltonian form, with general one-body and two-body interaction terms. We also presented details of the method in a way that facilitates efficient implementations, including advanced implementations which dramatically speed up the algorithm and reduce memory cost. We proposed the use of self-consistent constraints in molecules and solids, and studied the behavior under two different flavors.

The AFQMC method is very promising as a general computational method for strongly-correlated many electron systems. Many directions can be pursued in its development and application, for example, further reducing the scaling and improving the efficiency of the algorithm, computation of observables including imaginary-time correlations, finite-temperature AFQMC for materials and excited state calculations, etc. With increased attention and effort in the development of AFQMC both algorithmically and in software, many more applications can be expected in general material systems.

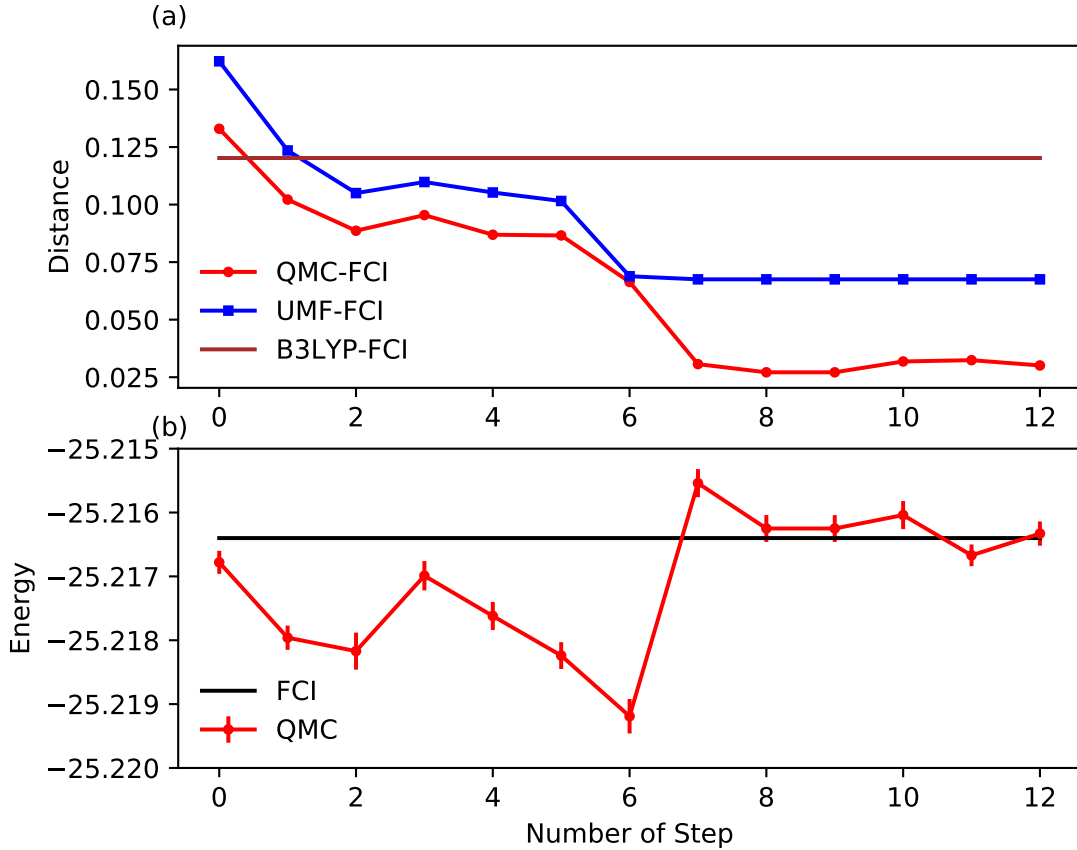


FIG. 4. Self-Consistent AFQMC optimization of an effective DFT Hamiltonian. The AFQMC calculation is coupled to an independent-electron calculation using an effective Hamiltonian resembling the B3LYP functional. The independent-electron calculation produces a single-determinant trial wave function for AFQMC, from which the computed density matrix is used to find a new effective Hamiltonian. Results are shown for the BH molecule in the *ccpVdZ* basis, versus self-consistent iteration steps. (a) The relative discrepancy of the computed one-body density matrices. The self-consistent iteration converges after 8 steps. Note that “DFT” (UMF) results also improve during the iteration. (b) AFQMC energy versus iteration.

VI. ACKNOWLEDGEMENTS

We acknowledge helpful discussions with Mario Motta, Wirawan Purwanto, and Mingpu Qin. The Flatiron Institute is a division of the Simons Foundation. This work was conducted using computational resources and services at the Flatiron Institute.

VII. DATA AVAILABILITY

The data that support the findings of this study are available from the corresponding author upon reasonable request.

REFERENCES

- ¹R. M. Martin, “Electronic structure: Basic theory and practical methods.” (Cambridge University Press, 2004).
- ²W. Kohn, “Nobel lecture: Electronic structure of matter—wave functions and density functionals,” *Rev. Mod. Phys.* **71**, 1253–1266 (1999).
- ³M. H. Kalos, D. Levesque, and L. Verlet, “Helium at zero temperature with hard-sphere and other forces,” *Phys. Rev. A* **9**, 2178–2195 (1974).
- ⁴W. M. C. Foulkes, L. Mitas, R. J. Needs, and G. Rajagopal, “Quantum monte carlo simulations of solids,” *Rev. Mod. Phys.* **73**, 33–83 (2001).
- ⁵D. M. Ceperley, “Path integrals in the theory of condensed helium,” *Rev. Mod. Phys.* **67**, 279–355 (1995).
- ⁶R. Blankenbecler, D. J. Scalapino, and R. L. Sugar, “Monte carlo calculations of coupled boson-fermion systems. i,” *Phys. Rev. D* **24**, 2278–2286 (1981).
- ⁷S. Zhang and H. Krakauer, “Quantum monte carlo method using phase-free random walks with slater determinants,” *Phys. Rev. Lett.* **90**, 136401 (2003).
- ⁸K. E. Schmidt and M. H. Kalos, “Few-and many-fermion problems,” in *Applications of the Monte Carlo Method in Statistical Physics*, edited by K. Binder (Springer Berlin Heidelberg, Berlin, Heidelberg, 1984) pp. 125–143.
- ⁹E. Y. Loh, J. E. Gubernatis, R. T. Scalettar, S. R. White, D. J. Scalapino, and R. L. Sugar, “Sign problem in the numerical simulation of many-electron systems,” *Phys. Rev. B* **41**, 9301–9307 (1990).
- ¹⁰S. Zhang, “Finite-temperature monte carlo calculations for systems with fermions,” *Phys. Rev. Lett.* **83**, 2777–2780 (1999).
- ¹¹S. Zhang, “Auxiliary-field quantum monte carlo for correlated electron systems,” (Verlag, 2013) Chap. Emergent Phenomena in Correlated Matter: Modeling and Simulation.

- ¹²W. A. Al-Saidi, S. Zhang, and H. Krakauer, “Auxiliary-field quantum monte carlo calculations of molecular systems with a gaussian basis,” *The Journal of Chemical Physics* **124**, 224101 (2006), <https://doi.org/10.1063/1.2200885>.
- ¹³M. Motta and S. Zhang, “Ab initio computations of molecular systems by the auxiliary-field quantum monte carlo method,” *WIREs Computational Molecular Science* **8**, e1364 (2018), <https://onlinelibrary.wiley.com/doi/pdf/10.1002/wcms.1364>.
- ¹⁴H. Hao, A. Georges, A. J. Millis, B. Rubenstein, Q. Han, and H. Shi, “Metal-insulator and magnetic phase diagram of Ca_2RuO_4 from auxiliary field quantum monte carlo and dynamical mean field theory,” *Phys. Rev. B* **101**, 235110 (2020).
- ¹⁵S. Zhang, J. Carlson, and J. E. Gubernatis, “Constrained path monte carlo method for fermion ground states,” *Phys. Rev. B* **55**, 7464–7477 (1997).
- ¹⁶H. Hao, B. M. Rubenstein, and H. Shi, “Auxiliary field quantum monte carlo for multiband hubbard models: Controlling the sign and phase problems to capture hund’s physics,” *Phys. Rev. B* **99**, 235142 (2019).
- ¹⁷H. Shi and S. Zhang, “Many-body computations by stochastic sampling in hartree-fock-bogoliubov space,” *Phys. Rev. B* **95**, 045144 (2017).
- ¹⁸M. Siewattana, W. Purwanto, S. Zhang, H. Krakauer, and E. J. Walter, “Phaseless auxiliary-field quantum monte carlo calculations with plane waves and pseudopotentials: Applications to atoms and molecules,” *Phys. Rev. B* **75**, 245123 (2007).
- ¹⁹F. Ma, W. Purwanto, S. Zhang, and H. e. Krakauer, “Quantum monte carlo calculations in solids with downfolded hamiltonians,” *Phys. Rev. Lett.* **114**, 226401 (2015).
- ²⁰M. Born and R. Oppenheimer, “Zur quantentheorie der molekeln,” *Annalen der Physik* **389**, 457–484 (1927), <https://onlinelibrary.wiley.com/doi/pdf/10.1002/andp.19273892002>.
- ²¹A. Szabo and N. Ostlund, “Modern quantum chemistry: Introduction to advanced electronic structure theory,” (Dover Publications, 1989).
- ²²N. H. F. Beebe and J. Linderberg, “Simplifications in the generation and transformation of two-electron integrals in molecular calculations,” *International Journal of Quantum Chemistry* **12**, 683–705 (1977), <https://onlinelibrary.wiley.com/doi/pdf/10.1002/qua.560120408>.
- ²³H. Koch, A. Snchez de Mers, and T. B. Pedersen, “Reduced scaling in electronic structure calculations using cholesky decompositions,” *The Journal of Chemical Physics* **118**, 9481–9484 (2003), <https://doi.org/10.1063/1.1578621>.

- ²⁴F. Aquilante, L. De Vico, N. Ferr, G. Ghigo, P.-. Malmqvist, P. Neogrady, T. B. Pedersen, M. Pitok, M. Reiher, B. O. Roos, L. Serrano-Andrs, M. Urban, V. Veryazov, and R. Lindh, “Molcas 7: The next generation,” *Journal of Computational Chemistry* **31**, 224–247 (2010), <https://onlinelibrary.wiley.com/doi/pdf/10.1002/jcc.21318>.
- ²⁵W. Purwanto, H. Krakauer, Y. Virgus, and S. Zhang, “Assessing weak hydrogen binding on Ca centers: an accurate many-body study with large basis sets,” *The Journal of Chemical Physics* **135**, 164105 (2011), <http://dx.doi.org/10.1063/1.3654002>.
- ²⁶J. Shee, E. Arthur, S. Zhang, D. Reichman, and R. Friesner, “Phaseless auxiliary-field quantum monte carlo on graphical processing units,” *Journal of Chemical Theory and Computation* **14** (2018), 10.1021/acs.jctc.8b00342.
- ²⁷P. R. C. Kent, A. Annaberdiyev, A. Benali, M. C. Bennett, E. J. Landinez Borda, P. Doak, H. Hao, K. D. Jordan, J. T. Krogel, I. Kynp, J. Lee, Y. Luo, F. D. Malone, C. A. Melton, L. Mitas, M. A. Morales, E. Neuscamman, F. A. Reboredo, B. Rubenstein, K. Saritas, S. Upadhyay, G. Wang, S. Zhang, and L. Zhao, “Qmcpack: Advances in the development, efficiency, and application of auxiliary field and real-space variational and diffusion quantum monte carlo,” *The Journal of Chemical Physics* **152**, 174105 (2020), <https://doi.org/10.1063/5.0004860>.
- ²⁸M. Motta, J. Shee, S. Zhang, and G. K.-L. Chan, “Efficient ab initio auxiliary-field quantum monte carlo calculations in gaussian bases via low-rank tensor decomposition,” *Journal of Chemical Theory and Computation* **15**, 3510–3521 (2019), PMID: 31091103, <https://doi.org/10.1021/acs.jctc.8b00996>.
- ²⁹M. Suzuki, “Relationship between d-dimensional quantal spin systems and (d+1)-dimensional ising systems equivalence, critical exponents and systematic approximants of the partition function and spin correlations,” *Prog. Theor. Phys.* **56**, 1454–1469 (1976).
- ³⁰H. F. Trotter, “On the product of semi-groups of operators,” *Proc. Am. Math. Soc.* **10**, 545–551 (1959).
- ³¹J. Hubbard, “Calculation of partition functions,” *Phys. Rev. Lett.* **3**, 77–78 (1959).
- ³²W. Purwanto and S. Zhang, “Correlation effects in the ground state of trapped atomic bose gases,” *Phys. Rev. A* **72**, 053610 (2005).
- ³³G. Sugiyama and S. Koonin, “Auxiliary field monte-carlo for quantum many-body ground states,” *Annals of Physics* **168**, 1 – 26 (1986).

- ³⁴J. E. Hirsch, “Two-dimensional hubbard model: Numerical simulation study,” *Phys. Rev. B* **31**, 4403–4419 (1985).
- ³⁵S. Sorella, S. Baroni, R. Car, and M. Parrinello, “A novel technique for the simulation of interacting fermion systems,” *Europhysics Letters (EPL)* **8**, 663–668 (1989).
- ³⁶S. R. White, D. J. Scalapino, R. L. Sugar, E. Y. Loh, J. E. Gubernatis, and R. T. Scalettar, “Numerical study of the two-dimensional hubbard model,” *Phys. Rev. B* **40**, 506–516 (1989).
- ³⁷H. Shi and S. Zhang, “Infinite variance in fermion quantum monte carlo calculations,” *Phys. Rev. E* **93**, 033303 (2016).
- ³⁸S. Zhang, “Auxiliary-field quantum monte carlo at zero- and finite-temperature,” (Verlag, 2019) Chap. Many-Body Methods for Real Materials.
- ³⁹D. Thouless, “Stability conditions and nuclear rotations in the hartree-fock theory,” *Nuclear Physics* **21**, 225 – 232 (1960).
- ⁴⁰D. Thouless, “Vibrational states of nuclei in the random phase approximation,” *Nuclear Physics* **22**, 78 – 95 (1961).
- ⁴¹H. Shi and S. Zhang, “Symmetry in auxiliary-field quantum monte carlo calculations,” *Phys. Rev. B* **88**, 125132 (2013).
- ⁴²H. Shi, C. A. Jiménez-Hoyos, R. Rodríguez-Guzmán, G. E. Scuseria, and S. Zhang, “Symmetry-projected wave functions in quantum monte carlo calculations,” *Phys. Rev. B* **89**, 125129 (2014).
- ⁴³J. Carlson, S. Gandolfi, K. E. Schmidt, and S. Zhang, “Auxiliary-field quantum monte carlo method for strongly paired fermions,” *Phys. Rev. A* **84**, 061602 (2011).
- ⁴⁴H. Shi, S. Chiesa, and S. Zhang, “Ground-state properties of strongly interacting fermi gases in two dimensions,” *Phys. Rev. A* **92**, 033603 (2015).
- ⁴⁵Y.-Y. He, M. Qin, H. Shi, Z.-Y. Lu, and S. Zhang, “Finite-temperature auxiliary-field quantum monte carlo: Self-consistent constraint and systematic approach to low temperatures,” *Phys. Rev. B* **99**, 045108 (2019).
- ⁴⁶J. P. F. LeBlanc, A. E. Antipov, F. Becca, I. W. Bulik, G. K.-L. Chan, C.-M. Chung, Y. Deng, M. Ferrero, T. M. Henderson, C. A. Jiménez-Hoyos, E. Kozik, X.-W. Liu, A. J. Millis, N. V. Prokof’ev, M. Qin, G. E. Scuseria, H. Shi, B. V. Svistunov, L. F. Tocchio, I. S. Tupitsyn, S. R. White, S. Zhang, B.-X. Zheng, Z. Zhu, and E. Gull (Simons Collaboration on the Many-Electron Problem), “Solutions of the two-dimensional hubbard

- model: Benchmarks and results from a wide range of numerical algorithms,” *Phys. Rev. X* **5**, 041041 (2015).
- ⁴⁷B.-X. Zheng, C.-M. Chung, P. Corboz, G. Ehlers, M.-P. Qin, R. M. Noack, H. Shi, S. R. White, S. Zhang, and G. K.-L. Chan, “Stripe order in the underdoped region of the two-dimensional hubbard model,” *Science* **358**, 1155–1160 (2017), <https://science.sciencemag.org/content/358/6367/1155.full.pdf>.
- ⁴⁸W. Purwanto and S. Zhang, “Quantum monte carlo method for the ground state of many-boson systems,” *Phys. Rev. E* **70**, 056702 (2004).
- ⁴⁹M. Motta and S. Zhang, “Computation of ground-state properties in molecular systems: Back-propagation with auxiliary-field quantum monte carlo,” *Journal of Chemical Theory and Computation* **13**, 5367–5378 (2017), pMID: 29053270, <https://doi.org/10.1021/acs.jctc.7b00730>.
- ⁵⁰G. C. Wick, “The evaluation of the collision matrix,” *Phys. Rev.* **80**, 268–272 (1950).
- ⁵¹R. Balian and E. Brezin, “Nonunitary bogoliubov transformations and extension of wick’s theorem,” *Nuovo Cim. B* **64**, 37–55 (1969).
- ⁵²J. Lee and D. R. Reichman, “Stochastic resolution-of-the-identity auxiliary-field quantum monte carlo: Scaling reduction without overhead,” *The Journal of Chemical Physics* **153**, 044131 (2020), <https://doi.org/10.1063/5.0015077>.
- ⁵³F. D. Malone, S. Zhang, and M. A. Morales, “Overcoming the memory bottleneck in auxiliary field quantum monte carlo simulations with interpolative separable density fitting,” *Journal of Chemical Theory and Computation* **15**, 256–264 (2019), <https://doi.org/10.1021/acs.jctc.8b00944>.
- ⁵⁴B. K. Clark, M. A. Morales, J. McMinis, J. Kim, and G. E. Scuseria, “Computing the energy of a water molecule using multideterminants: A simple, efficient algorithm,” *The Journal of Chemical Physics* **135**, 244105 (2011), <https://doi.org/10.1063/1.3665391>.
- ⁵⁵Q. Sun, T. C. Berkelbach, N. S. Blunt, G. H. Booth, S. Guo, Z. Li, J. Liu, J. D. McClain, E. R. Sayfutyarova, S. Sharma, S. Wouters, and G. K.-L. Chan, “Pyscf: the python-based simulations of chemistry framework,” *WIREs Computational Molecular Science* **8**, e1340 (2018), <https://onlinelibrary.wiley.com/doi/pdf/10.1002/wcms.1340>.
- ⁵⁶K. T. Williams, Y. Yao, J. Li, L. Chen, H. Shi, M. Motta, C. Niu, U. Ray, S. Guo, R. J. Anderson, J. Li, L. N. Tran, C.-N. Yeh, B. Mussard, S. Sharma, F. Bruneval, M. van Schilfgaarde, G. H. Booth, G. K.-L. Chan, S. Zhang, E. Gull, D. Zgid, A. Millis, C. J.

- Umrigar, and L. K. Wagner (Simons Collaboration on the Many-Electron Problem), “Direct comparison of many-body methods for realistic electronic hamiltonians,” *Phys. Rev. X* **10**, 011041 (2020).
- ⁵⁷J. Shee, B. Rudsteyn, E. J. Arthur, S. Zhang, D. R. Reichman, and R. A. Friesner, “On achieving high accuracy in quantum chemical calculations of 3d transition metal-containing systems: A comparison of auxiliary-field quantum monte carlo with coupled cluster, density functional theory, and experiment for diatomic molecules,” *Journal of Chemical Theory and Computation* **15**, 2346–2358 (2019), pMID: 30883110, <https://doi.org/10.1021/acs.jctc.9b00083>.
- ⁵⁸B. Rudsteyn, D. Coskun, J. L. Weber, E. J. Arthur, S. Zhang, D. R. Reichman, R. A. Friesner, and J. Shee, “Predicting ligand-dissociation energies of 3d coordination complexes with auxiliary-field quantum monte carlo,” *Journal of Chemical Theory and Computation* **16**, 3041–3054 (2020), pMID: 32293882, <https://doi.org/10.1021/acs.jctc.0c00070>.
- ⁵⁹C.-C. Chang, B. M. Rubenstein, and M. A. Morales, “Auxiliary-field-based trial wave functions in quantum monte carlo calculations,” *Phys. Rev. B* **94**, 235144 (2016).
- ⁶⁰M. Qin, H. Shi, and S. Zhang, “Coupling quantum monte carlo and independent-particle calculations: Self-consistent constraint for the sign problem based on the density or the density matrix,” *Phys. Rev. B* **94**, 235119 (2016).
- ⁶¹Y. Virgus, W. Purwanto, H. Krakauer, and S. Zhang, “Stability, energetics, and magnetic states of cobalt adatoms on graphene,” *Phys. Rev. Lett.* **113**, 175502 (2014).
- ⁶²M. Motta, D. M. Ceperley, G. K.-L. Chan, J. A. Gomez, E. Gull, S. Guo, C. A. Jiménez-Hoyos, T. N. Lan, J. Li, F. Ma, A. J. Millis, N. V. Prokof’ev, U. Ray, G. E. Scuseria, S. Sorella, E. M. Stoudenmire, Q. Sun, I. S. Tupitsyn, S. R. White, D. Zgid, and S. Zhang (Simons Collaboration on the Many-Electron Problem), “Towards the solution of the many-electron problem in real materials: Equation of state of the hydrogen chain with state-of-the-art many-body methods,” *Phys. Rev. X* **7**, 031059 (2017).
- ⁶³M. Motta, C. Genovese, F. Ma, Z.-H. Cui, R. Sawaya, G. Kin-Lic Chan, N. Chepiga, P. Helms, C. Jimenez-Hoyos, A. J. Millis, U. Ray, E. Ronca, H. Shi, S. Sorella, E. M. Stoudenmire, S. R. White, and S. Zhang (Simons Collaboration on the Many-Electron Problem), “Ground-state properties of the hydrogen chain: insulator-to-metal transition, dimerization, and magnetic phases,” *Phys. Rev. X* **10**, 031058 (2020).